Surfaces and Interfaces 31 (2022) 101975

Contents lists available at ScienceDirect

Surfaces and Interfaces

journal homepage: www.sciencedirect.com/journal/surfaces-and-interfaces

Ti and TiO_2 magnetron sputtering in roll-to-roll fabrication of hybrid membranes

Arnoux Rossouw [a,b,*], Andrzej Olejniczak [a,e], Katarzyna Olejniczak [a,e], Boris Gorberg [d], Iliya Vinogradov [a,c], Olga Kristavchuk [a], Alexander Nechaev [a,c], Leslie Petrik [f], Willem Perold [b], Sergey Dmitriev [a]

[a] Joint Institute for Nuclear Research, St. Joliot-Curie 6, Dubna, Moscow Region, 141980 Russia
[b] Faculty of Engineering, Stellenbosch University, Stellenbosch 7602, South Africa
[c] Dubna State University, St. Universitetskaya 19, Moscow Region 141980 Russia
[d] Ivanovo State University of Chemistry and Technology, Sheremetevskii pr. 7, Ivanovo 153000 Russia
[e] Faculty of Chemistry, Nicolaus Copernicus University, St. Gagarina 7, Torun 87-100, Poland
[f] Department of Chemistry, University of the Western Cape, Cape Town 7535, South Africa

ARTICLE INFO

Keywords:
Titanium dioxide
Roll-to-roll
Magnetron sputtering
Thin film
Surface modification
Track etched membrane

ABSTRACT

The large-scale surface modification of polyethylene terephthalate track-etched membranes (TM) using industrial roll-to-roll planar magnetron sputtering of Ti and TiO_2 for use in advanced technologies such as separation, biotechnology, and microelectronics was investigated. The Ti and TiO_2-Ti coated TM surface characterisation was done using a combination of scanning electron microscopy, atomic force microscopy, contact angle- and scratch adhesion testing. Structural characterisation was done using transmission electron microscopy, energy dispersive x-ray spectroscopy, x-ray photoelectron spectroscopy, and tensile testing. Water permeability and bubble point testing were used to confirm the membrane permeability after surface modification. A tensile test showed that the coated membranes' strength was within an acceptable range of one another. Magnetron sputtering did not lead to significant changes in the water permeability, nor a notable reduction in the pore diameter of the resulting Ti-TM and TiO_2-Ti-TM hybrid membranes. Sputtered coatings on top of the TM surface significantly reduced the water contact angle from 72° for an untreated TM to 33° and 28° for Ti-TM and TiO_2-Ti-TM, respectively. This investigation shows that roll-to-roll magnetron sputtering is a viable approach to the large-scale fabrication of hybrid membranes based on TM as model support.

1. Introduction

Track- or track-etched membranes (TM) as a porous system with high uniformity of pore size and shape have extensive prospects for use in various membrane processes related to biotechnology, ecology, medicine and analytical chemistry [1,2]. The use of surface modification methods is one of the most effective approaches to solving the problem of improving the properties of membranes and creating porous functional polymer systems with tailored structural and physicochemical properties.

To date, numerous works have been devoted to the development of methods for modifying TM surfaces [3–6]. These methods can be divided into two primary groups: firstly, methods consisting of applying a low- or high-molecular compound to the surface of the membrane, thereby forming a layer with predetermined properties, and secondly, methods that include changing the physicochemical properties of the near- or outer-surface layer of the polymer membrane.

The methods of TM modification of the first group include plasma-, radiation-, and chemical grafting, polymerisation, modification by physical or chemical adsorption, and chemical grafting of various high-molecular compounds [3,4]. The advantages of the methods of this group include a wide variety of processing options and a vast range of substances that can be used for modification. Therefore, these methods are usually used to synthesise TMs with specific properties in order to fulfil their intended tasks.

The second group mainly consists of treating membranes in the plasma of ionised gases or the vapours of strong oxidants [4,6]. These methods are generally used to clean the surface of track membranes or to

* Corresponding author at: Joint Institute for Nuclear Research, St. Joliot-Curie 6, Dubna, Moscow Region, 141980 Russia.
E-mail address: rossouw@jinr.ru (A. Rossouw).

https://doi.org/10.1016/j.surfin.2022.101975
Received 9 August 2021; Received in revised form 3 February 2022; Accepted 11 April 2022
Available online 14 April 2022

increase their hydrophilicity. The main advantage of these methods is their versatility: they can be used to treat the surface of membranes made from various types of polymers with practically any pore diameter.

However, high-tech solutions for modern ion-plasma processing methods have brought about new, more effective approaches to the surface modification of various polymer materials [7]. One such approach is to modify the surface of non-porous polymer films by applying a thin coating of metal or ceramic directly to the polymer's surface. Magnetron sputtering occupies a niche sector [8–10], and it allows for the alteration of both the structure and composition of the outermost surface of the material. Consequently, this affects various surface characteristics such as adhesion, wettability, and biocompatibility, without changing the bulk properties [11–15].

Magnetron sputtering offers numerous advantages, such as the option to deposit metals, ceramics, and polymer thin films. The deposition rate can be varied, and the sputtered films' properties can be tailored by changing one or more deposition parameters such as power, pressure, and gas composition. This allows for the deposition of high purity films with good adhesion to the polymer supporting membrane. Additionally, it is possible to construct semicontinuous process lines due to the nature of the target materials [16–18].

Currently, magnetron sputtering is not being used for large-scale surface modification of porous polymeric membranes. This is primarily due to the difficulty in manufacturing and implementing high-vacuum equipment for the industrial surface modification of porous polymeric membranes. There are complications to be dealt with, both scientific- and engineering-related, before the viable implementation of this approach in the industry. Fortunately, advancements in low-pressure plasma treatment technology of textile materials have made the sputter coating of porous polymeric membranes a more realistic endeavour [19].

The Flerov Laboratory of Nuclear Reactions at the Joint Institute for Nuclear Research (JINR), together with the company Ivtechnomash LLC, has carried out extensive research and development on the use of magnetron sputtering for the modification of textiles and track membranes. With a particular focus on the influence of the process parameters (discharge current, pressure, gas composition) and the target material on the sputter deposition rate, composition and properties of the resulting coatings. Thin films of aluminium, titanium, copper, silver and stainless steel on polymer films were obtained using planar magnetron sputtering on a laboratory scale installation [17].

This paper presents the possible application of industrial magnetron sputtering for the surface modification of polymer membranes. Titanium (Ti) was chosen as the target material and from it both Ti and TIO_2 was sputtered on top of the TM support. On the one hand, Ti is an inert metal with good electrical conductivity, exceptional chemical resistance, thermal stability, high hardness, a high melting point and results in a low number of crystallographic defects when used for sensitive electrodes, buffer or adhesive layers [18,20]. On the other hand, TiO_2 is one of the most promising catalysts because of its extensive range of applications and the relative ease with which it can be implemented in mass production [17,21–28]. Upgrading the membrane filtration technology using TM is an attractive solution for applications that currently use TMs. It is anticipated that hybrid TMs with a metallised surface layer will be used in electrospinning nanofibers on their surface and in creating the next generation of membrane-sorption materials. Thus, the motivation of this study is to propose approaches and technological solutions for modifying the surface of TMs by developing a large-scale magnetron sputtering process for future applications as an effective method for functionalising their surfaces.

2. Experimental

2.1. Ti and TiO_2 thin-film deposition

Samples were made from Hostaphan RNK PET film, 23 μm thick, 320 mm wide and 100 m long, manufactured by Mitsubishi Polyester Films. According to the manufacturer, the film is produced by co-extrusion from a melt stream and consists of an inner layer free from filler particles and thin outer layers of polymer containing a small additive of nanodispersed silicon dioxide. During production, the film is subjected to biaxial drawing and subsequent heat treatment, which forms a semi-crystalline polymer structure. The density of the film material is 1.4 g/cm^3. Irradiation using a $^{132}Xe^{+26}$ beam was done at a specific energy of 1.16 MeV/amu and 90°±30° angle to the normal from one side using the IC-100 cyclotron at FLNR JINR. The surface density of pores on each side was $N = 2.7 \pm 0.3 \times 10^8$ cm^{-2}. Before etching, all samples were exposed to UV radiation at a rate of 25 m/hr. The 0.3 μm diameter pores were characterised in FLNR using the bubble point method, and the porosity of the membrane was determined to be between 10 and 15%. An in-depth review of the complete TM fabrication method was reported by Flerov et al. [29] and Apel and Dmitriev [30].

Despite not finding any literature on industrial-scale sputtering on top of TMs, this deposition was made possible by using the UMN-180 planar magnetron sputtering unit developed by "Ivtekhnomash" LLC, see Fig. 1 for a schematic of the device. The UMN-180 machine is equipped with a 2088 mm long magnetron sputtering unit, which allow uniform-thickness coatings to be deposited with an accuracy of ±10% on fabrics up to 180 cm in width. The two-step vacuum system evacuates air from the working chamber loaded with a roll of fabric or film (residual pressure 5×10^{-5} mm Hg). The accuracy of maintaining the flow and pressure of the working gas (or gas mixture) during treatment is ±5%. The machine is equipped with auxiliary cooled electrodes to excite glow discharge to activate the surface before coating deposition. The conveyor system uniformly pulls the material through the plasma treatment and coating deposition zone at a 20 m/min rate and is adapted for textile fabrics as well as polymer films, with a thickness between 12 μm and 7 mm [31]. See Table 1 for a list of the sputtering parameters.

For the modification of TMs using Ti and TiO_2, the following approach was used: Before sputtering, the TM needs to be cleaned to deposit metals and oxide layers successfully. After air plasma-chemical pre-treatment of the TM surface, a thin film of Ti was sputtered on top of the TM surface. TM surface metallisation can be identified as a significant commercial product as well as providing a sub-layer or precursor for TiO_2 deposition with good adhesion. Sputter deposition was uniform over the length of the TM roll. This was due to the Ti target being 6x wider than the film. This work exhibited good resistance to dry friction and wet wiping of sputtered coatings on polyester membranes, provided that it was subjected to pre-treatment and contained no particles or lubricant residues. Plasma chemical surface pre-activation enhanced the adhesion of metal nanofilms to the polymer material 2–3 times [32]. Deposition parameters for Ti and TiO_2 were optimised for this experiment; however, the optimisation method will not be presented here as it is not the focus of this article.

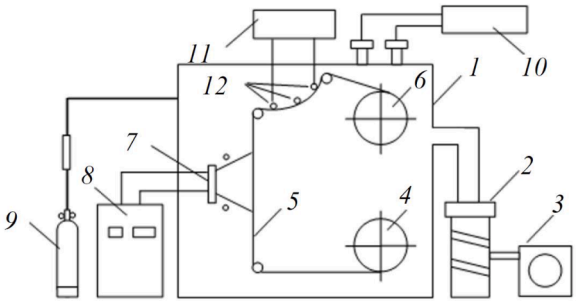

Fig. 1. Schematic of the UMN-180 magnetron sputtering machine–(1) Vacuum chamber; (2) diffusion pump; (3) fore vacuum pump; (4) collector roll; (5) coated material; (6) distributor roll; (7) magnetron; (8) magnetron power supply unit; (9) argon inlet system; (10) reactive gas inlet system; (11) power supply unit for the plasma cleaning; and (12) plasma cleaning system.

Table 1
Sputter deposition parameters for the UMN-180 system.

Parameter	Units
"Spot" size	0.3 m x 1.8 m
Max roll diameter	0.7 m
Volume of evacuated chamber	15 m^3
Number of magnetrons	1
Working pressure	7×10^{-3} Pa
Current	16 A
Processing speed	0–20 m/min

PET TMs are made up of a mixture of amorphous and crystalline particles ~20–30 nm in size. Therefore, it was decided to sputter 40 nm (±10%) of Ti base layer to ensure the TM surface's complete coating. Following the Ti sublayer deposition, approximately 40 nm (±10%) of TiO_2 was sputtered on top of it. The coating covers the entire Ti-TM surface at this thickness, including any possible crevasses or defects without filling in the TM pores or resulting in any cracks or loss of thin-film durability and adhesion, see Fig. 2.

2.2. Ti and TiO_2 thin-film characterisation

The surface morphology was investigated using a SU-8020 high-resolution field-emission SEM (Hitachi, Japan). Element distributions for C, N_2, O_2 and Ti were examined using the attached Oxford Instruments Aztec Energy energy dispersive spectroscopy Analysis System (EDS) at an accelerating voltage between 3 and 10 kV.

Further structural characterisation was done on a Ntegra (NT-MDT, Russia) atomic force microscope (AFM) operating in tapping mode using NSG10 cantilever tips. After sputtering Ti and TiO_2 on top of silicon wafers, the average deposition rate was determined by measuring the film thickness by AFM and dividing it by the time taken to deposit the films. Silicon wafers were chosen for this purpose as they are much more robust than TMs and the difference in the resulting deposition rate was negligible.

TEM structural studies were carried on a JEOL JEM-2100 high-resolution electron microscope.

XPS of Ti-TM and Ti-TiO_2-TM specimens were acquired on a K-alpha (Thermo Fisher) spectrometer with a monochromatized X-ray source (Al Kα, 1486.68 eV). All spectra were charge referenced to the deconvoluted Ti 2p3/2 peak of TiO_2 at 458.6 eV. The spectral acquisition parameters and deconvolution procedure were described elsewhere [33].

Fig. 2. Photo of TiO_2-Ti-TM (goldish), Ti-TM (silverish) and TM (whitish) rolls.

Throughout the paper, we use a line shape notation policy in accordance with CasaXPS software. Namely, the GL(x) line denotes a Gaussian/-Lorentzian product with the mixing factor x equal to 100 for pure Lorentzian and 0 for pure Gaussian. LA (α, β, m) represents a convolution of a Lorentz line with a Gaussian of width m; where α and β specify the tail's spread, respectively, on the low- and high binding energy (BE) side of the Lorentz curve. The depth profiling was performed with a beam of 2 keV monoatomic Ar+ ions rastered over an area of 1 × 1 mm^2 (5x more extensive than an X-ray spot). For this investigation, films of equal thickness were investigated. Ti deposition time for a Ti-TM was doubled, resulting in an 80 nm Ti-TM and an 80 nm TiO_2-Ti-TM (40 nm TiO_2 and 40 nm Ti).

In order to evaluate the adhesion of the coatings and their resistance to scratching from critical loads at which the coatings break down and/or peels off, the scratch-test method (controlled scratching), was done using a scratch tester with micro- (MST) and nano- (NST) modules based on the open platform OPX (CSM Instruments) that allows testing of samples with coatings. During the controlled scratch test of Ti and TiO_2-Ti coated TMs for evaluating the adhesive properties of the coatings, the load application increased linearly at a rate of 100 mN/min from 2 mN (min) to 52 mN (max). The length of the scratch was 500 μm and the diamond conical-sphere indenter has a 2 μm radius and was applied at a 90° angle.

The tensile mechanical properties of the investigated films were measured at room temperature using a Shimadzu AGS-X testing machine equipped with a 50 N load cell. Samples of rectangular shape with a width and a gauge length of 10 and 40 mm, respectively, were stretched at a rate of 1 mm/min. The sample thickness was measured by a Labthink C640 thickness tester. The stress and strain parameters were calculated using the Trapezium X software. Average values and standard deviations for both parameters were determined from 6 independent measurements.

Using a Krüss DSA100 Drop shape analysis System (Krüss GmbH, Germany), contact-angle measurements were carried to analyse the hydrophilic effect of the surface metallisation of the TMs. Droplets of deionised water are carefully placed on top of the sample surface (3 mL, room temperature, 18.2 MOhm cm, Milli-Q Advantage A10, Millipore, USA). After that, the acquisition of an image of the droplet and the following calculation of both contact-angles (left and right) was made using the DSA4 (Krüss GmbH, Germany) software. This is also known as the sessile or recumbent drop method.

Membrane permeability and pore size determination was done by utilising a combination of SEM, water permeability and bubble-point tests. The measurement of pores' diameter by the bubble point method was carried out using a POROLUX 1000. This method is used to determine the size of the largest pore of the samples. A sample is loaded into the working chamber, moistened with liquid and then the chamber is sealed. After that, gas is introduced from one side of the chamber and will result in a linear pressure increase in the sample chamber. When the first pore opens, there will be a sudden change in line pressure. The bubble point pressure is the pressure at which the first derivative will begin to deviate from a straight line.

3. Results and discussions

For a deeper understanding of the hybrid membranes created by sputter coating, thin films of metallic-Ti and ceramic-TiO_2 on top of a TM support, and the deposited thin films' physicochemical properties, both the structural and mechanical characteristics were investigated.

3.1. Scanning electron- and atomic force microscopy

The surface morphology of the Ti and TiO_2-Ti thin films were investigated by SEM, see Fig. 3. After Ti sputtering the post-deposition surface topography remained similar to that of the native track etched membrane, see Fig. 3a-b. However, despite the pores retaining a mostly

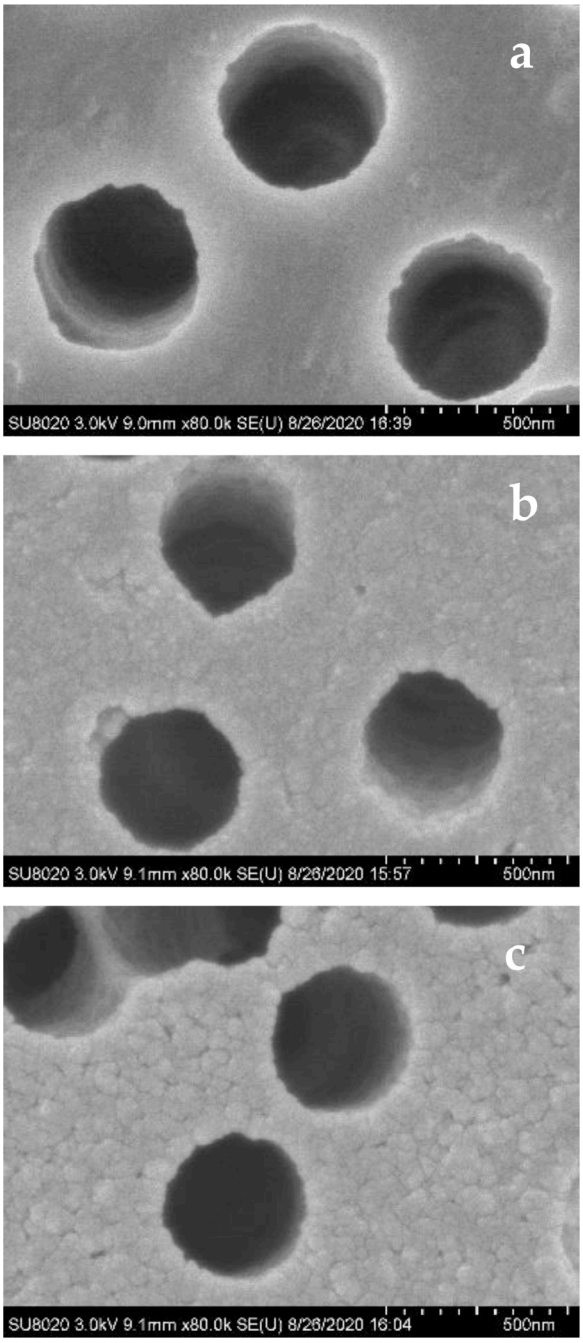

Fig. 3. SEM micrographs of a) TM, b) Ti-TM, c) TiO_2-Ti-TM.

circular shape, a reduction in pore the diameter was noticed. The 40 nm (±10%) of Ti sputtered on top of the native TM surface reduced the surface pore diameter from 0.45 μm to approx. 0.42 μm.

After sputtering the 40 nm (±10%) of TiO_2 on top of the Ti coated TM, see Fig. 3c, the pore shape did not change, however the surface diameter of the pores reduced slightly more, from the original 0.45 μm to approx. 0.39 μm. In contrast to the lab-scale results, see [33], there were no occlusion of the pores occurring. Nonetheless, upon closer examination double pores, formed by two swift heavy ions crisscrossing the PET film during ion irradiation, when seen from afar, could be mistaken as elongated narrow pores after sputtering Ti and TiO_2, see top left-hand corner of Fig. 3c. To avoid any confusion, it is essential to note that despite the SEM surface pore diameter measured being much larger than the 0.3 μm stated in experiments and methods, TM pore dimension data sheets are based on bubble point measurements as the pores have an hourglass shape due to the way they are formed.

The surface topography of the thin films was further investigated by atomic force microscopy. AFM effectively measures the coating thickness and surface roughness. The deposition rate was determined through sputtering Ti and TiO_2 coatings on top of silicon wafers as it was not possible to create a reliable step-edge for AFM measurement on the TMs. The sputtered metallic Ti was approximately 40 nm thick, Fig. 4a, deposited at a rate of 0.36 nm/s, and the ceramic TiO_2 was approximately 40 nm thick, Fig. 4b, deposited at a rate of 0.18 nm/s. Only sections between the TM pores were chosen for AFM measurements to avoid pore influence and false profiles. The average roughness for the native TM can be found elsewhere [33].

The Ti and TiO_2 coatings sputtered on the TMs had a normal height difference between 5 and 20 nm. It could be because the coated TMs retained some similarity to the hillock-like structure of the underlying TM support [34]. As seen in Fig. 4c-d, the exterior of the coated TMs shows the presence of nanocrystallites or nanofibrils with relatively uniform sizes and spatial distribution [35–37]. Such surface morphology is developed due to physicochemical etching of the PET film after ion irradiation. The grain size distribution seems more consistent in the TiO_2-Ti-TM sample (Fig. 4d) than in the Ti-TM sample (Fig 4c). It is most likely due to the Ti being the first coating, thereby taking the shape of the TM surface, whereas TiO_2 has a Ti seed layer to attach to and forms smaller crystalline clusters as the film thickens out.

Nonetheless, the larger grains seem to be composed of smaller particles for Ti and TiO_2-Ti samples, which is beneficial for applications where an increased surface area benefits processes such as catalysis. The fine grain size should also reduce cracking susceptibility during solidification [38].

3.2. *Transmission electron microscopy*

The morphology, composition, and crystallography of the Ti and Ti-TiO2 thin films on top of their TM supports were investigated using TEM.

The deposited thin films, Ti and Ti-TiO_2, were separated from their PET TM support by dissolving the latter in a hot NaOH solution. Thiswas accomplished by floating the membrane on top of the NaOH solution. Doing so minimises the effect of the solution on the coatings themselves, especially the upper part that will be measured. The dissolution of the TM support is necessary. Otherwise, the sample would be too thick for the TEM investigation.

The detached coatings, see Fig. 5, were continuous but of variable thickness and heterogeneous due to the separation technique, as can be seen in Fig. 5a. As a result, the areas suitable for viewing were limited, and it was impossible to obtain diffraction patterns for all fields of view. However, the typical microstructure of the areas from which diffraction patterns were obtainable gave grounds to affirm that the microdiffraction is typical for Ti and TiO_2, see Fig 6.

The “holes” visible in Fig. 5a correspond to the pores of the dissolved TM and are close to 0.3 μm. Some remnants of the undissolved PET TM can be seen in the lower part of Fig. 5b. amongst the separated Ti films, Ti that partially coated the inner walls of the pores of the track membrane can be made out as tubes of up to 1 μm in length with a diameter of ~0.3 μm. This is interesting to note, especially for investigations into nanotube synthesis.

The electron diffraction pattern of the Ti-TM shown in Fig. 6a is homogeneous and consists of small crystallites with a characteristic grain size of ~ 5 nm. The diffraction pattern obtained is typical for polycrystalline materials consisting of small crystallites with a random orientation. Analysis of the crystal lattice showed that the structure of the titanium coating consisted almost exclusively of the fcc phase (space group Fm3m) with $a \approx 0.417$ nm. The film’s actual composition is not Ti (metallic) but the oxide of the composition ~ TiOx with a 50–54 atomic percentage O.

Fig. 6b shows the electron diffraction pattern for TiO_2-Ti-TM. It has

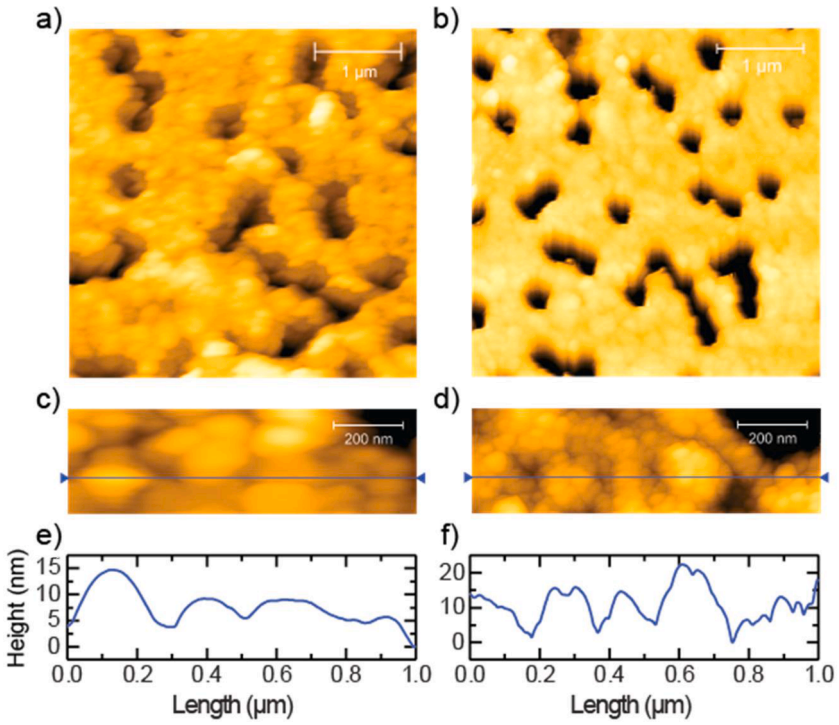

Fig. 4. AFM images of Ti-TM (left) and TiO_2-Ti-TM (right) films deposited by magnetron sputtering (a-d) along with height profiles extracted along the blue lines (e, f).

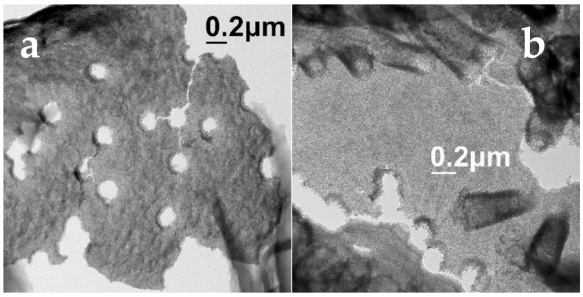

Fig. 5. TEM micrographs of a) Ti coating separated from TM (left), b) Ti "tubes" from TM pores (right).

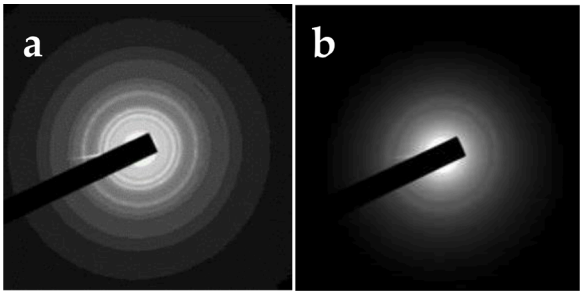

Fig. 6. Electron diffraction pattern after removal of the TM for Ti-TM (a) and TiO_2-Ti-TM (b).

very diffuse rings, indicating an isotropic fine-grained, ≤5 nm structure containing some amorphous component. In addition to the amorphous phase, the coating contains a nanocrystalline phase with the structure of anatase and/or the hexagonal phase of TiO_2.

3.3. *X-ray photoelectron spectroscopy and energy dispersive X-ray spectroscopy*

The XPS technique was employed to study the surface chemical compositions and perform elemental depth profiling of the TiO_2-Ti-TM and Ti-TM films. The Ti 2p spectra collected at the surfaces of both specimens are shown in Fig. 7. It is noteworthy that the TiO_2-Ti-TM specimen obtained by laboratory-scale magnetron sputtering [33] consisted only of TiO_2 and a single pair of symmetric lines (GL for $j = 3/2$ and LA for $j = 1/2$) was sufficient to deconvolute the spectrum. However, for the industrial-scale TiO_2-Ti-TM, such a simple model did not suffice, and the residual values at low binding energy sides of TiO_2 2p 1/2 and 3/2 components were relatively high. An additional pair of peaks at 457.2 eV (2p3/2) and 462.92 eV (2p1/2) was necessary to obtain a satisfactory fit (Fig. 7b). These peaks were attributed to Ti(III) oxide. Based on their integrated intensities, the atomic raTiO of Ti-bound in TiO_2 to that in Ti_2O_3 was ~18.3:1 (94.8 at.% and 5.2 at.%, respectively). Some authors suggested that the broadening of TiO_2

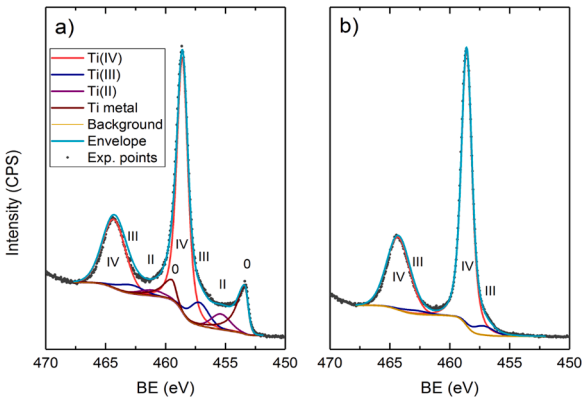

Fig. 7. Ti 2p core level spectra recorded on the surface of (a) Ti-TM and (b) TiO_2-Ti-TM specimens.

2p3/2 signal at low BE side could be related to defects in TiO_2 crystal [39]. This interpretation also coincides with the disordered nano-crystalline structure of the sputtered layer.

Ti 2p core level surface spectrum of the Ti-TM film (Fig. 7a) was complex, suggesting various Ti oxides and metallic Ti. Its deconvolution with spin-orbit splitting set to 5.7 eV for oxides and 6.03 eV for Ti(0) [40] yielded four pairs of peaks. These were attributed to TiO_2 (BE Ti2p3/2 = 458.6 eV), Ti_2O_3 (BE Ti2p3/2 = 457.2 eV), TiO (BE Ti2p3/2 = 455.4 eV), and metallic Ti (BE Ti2p3/2 = 453.8 eV). Similarly, as in the case of the corresponding specimen obtained in the lab-scale process [41], the main component was TiO_2 rather than metallic Ti. The atomic raTiO of Ti bound in TiO_2: Ti_2O_3: TiO: Ti(0) was 4.64:0.63:0.42:1 (69.3%, 9.4%, 6.3%, and 14.9%). These results point out that for industrial-scale process the formation of high oxidation state Ti oxides (TiO_2 and Ti_2O_3) is favoured at the expense of low oxidation state species (TiO and Ti^0), as found in the lab-scale process.

The bulk composition of the sputtered films was investigated by XPS depth profiling technique employing an Ar+ beam of 2 keV energy (Fig. 8). A drawback of etching with monoatomic ions of this energy range is that titanium oxides undergo a gradual reduction, and the polymer substrate suffers from deoxygenation. These deleterious effects made determining the actual chemical compositions of the magnetron sputtered layers barely possible.

Thus, we only considered changes in elemental concentrations and extracted depth profiles of some stable species. The elemental depth profiles obtained for both films are shown in Fig. 8a-b. Both specimens were covered by a thin overlayer of a carbonaceous contaminant that was easily removed during the ion etching. For Ti-TM specimen (Fig. 8a), Ti atoms' content was relatively constant (~ 35 at.%) throughout the whole magnetron sputtered layer. At the same time, the content of O atoms gradually decreased. This change was accompanied by an evolution in high-resolution Ti2p spectra, pointing out the occurrence of ion-beam induced reduction of titanium oxides (so-called preferential sputtering). Additional etching cycles, carried out after reaching the TM surface, showed that Ti concentration was still significant (7–8 at.%), and it started to decrease slowly only after as many as 300 cycles (~ 3000 s). This result is in line with a direct HR-TEM observation showing the presence of relatively long (~ 0.8 um) titanium nanotubes grown in the pores (Fig. 5b – TEM image).

In the case of TiO_2-Ti-TM, a distinct transition in the elemental composition between TiO_2 and Ti sputtered layers was visible, (Fig. 8b). The initial O/Ti raTiO was ~ 2:1, confirming the presence of TiO_2 in the top layer. However, the second layer was more oxygen-deficient (O/Ti of ~1). A pronounced difference between Ti-TM and TiO_2-Ti-TM was visible for the oxygen concentration profile in the proximity of the Ti| TM interface. In the first case, once the sputtered layer is etched, O content decreases monotonically, whereas in the second case O level initially increases after the TM surface is reached.

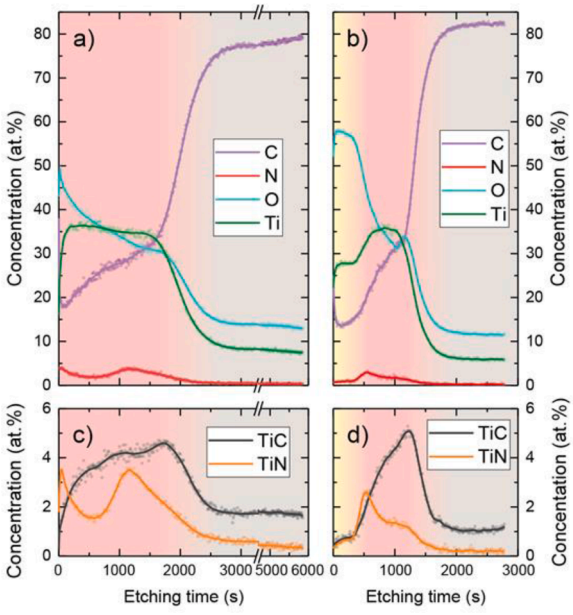

Fig. 8. XPS concentration depth profiles for (a,c) Ti-TM and (b,d) TiO_2-Ti-TM specimens.

Deconvolution C1s and N1s spectra allowed the extraction of the concentration depth profiles of TiN and TiC (Fig. 8c, d). The C1s line of TiC (282 eV) and N1s line of TiN (397 eV) were asymmetric. The origin of asymmetry in the first case lies in interface/disorder effects [42] while in the second case is due to the presence of titanium oxynitride (TiNO) [43]. For both films, the maximum content of TiC occurs at the interface of the sputtered Ti layer and TM. This result, along with the unexpected carbon contamination, suggests that the TM surface's partial decomposition occurs during Ti sputtering. The surface decomposition would also account for the origin of the TiC interfacial layer formed between the TM support and Ti coating.

Along the Ti layer the content of TiC varies in proportion to the total atomic concentration of carbon. In Fig. 8d the concentrations of both TiC and TiN are much lower for the TiO_2 sputtered layer. For the TiO_2-Ti-TM (Fig. 8d) the maximum in TiN concentration is shifted towards the TiO_2/Ti interface, giving the film its distinctive golden appearance. An increased level of TiN is also visible at the portion of the concentration profile representing the near-surface layer (etch time 0–350 s) of Ti-TM film. In this case, however, the TiN content might be overestimated. N1s spectra recorded in this etch time interval reveal other N species; the signal at ~ 397 eV is much broader, suggesting a possible coincidence with other N forms. See Fig. 9 for a graphical cross section depicting the sputtered films.

Energy dispersive spectroscopy (EDS) measurements were done at an electron acceleration voltage of 10 kV. At this acceleration voltage, the electrons' penetration depth is approximately—1000 nm, exceeding the sputtered Ti and TiO_2 film thickness. Consequently, a substantial share of the EDS signal originates from the underlying polymer support, and the EDS results can only be used in a qualitative and not quantitative capacity. Nevertheless, EDS did detect the presence of Ti, O, C, and N, which was consistent with the XPS depth profiling.

The composition of a thin film being deposited in a semi-controlled, low-vacuum environment is very precarious as it can be influenced by a multitude of uncertainties. In this case the substrate and the degassing thereof played a significant role and resulted in altering the composition of a significant portion of the film during sputter deposition. Further investigation into this phenomenon is advised.

3.4. Scratch test

Based on the resulting data of scratches, changes in measured loads corresponding to different stages of coating destruction were determined, and the coefficient of friction at critical load is presented in Table 2.

The destruction of the coating on the studied samples occurred on average at a load of 3.8–8.6 mN. Small critical loads are most likely due to the low hardness of the TM support. The greatest strength is observed in the "narrow strip" seen in Fig. 10a of sample Ti-TM at an average critical load of 8.6 mN, however, in the "wide strip" seen in Fig. 10b and Fig. 11b of these samples, the coating breaks down almost immediately (in the average load of 3.8–3.9 mN).

3.5. Tensile test

The stress-strain curves registered for pristine PET films, PET track-etched membranes, and those coated by titanium and both titanium and titanium dioxide are shown in Fig. 12. The shape of the curves obtained for the pristine and metallized PET films differs from the shape

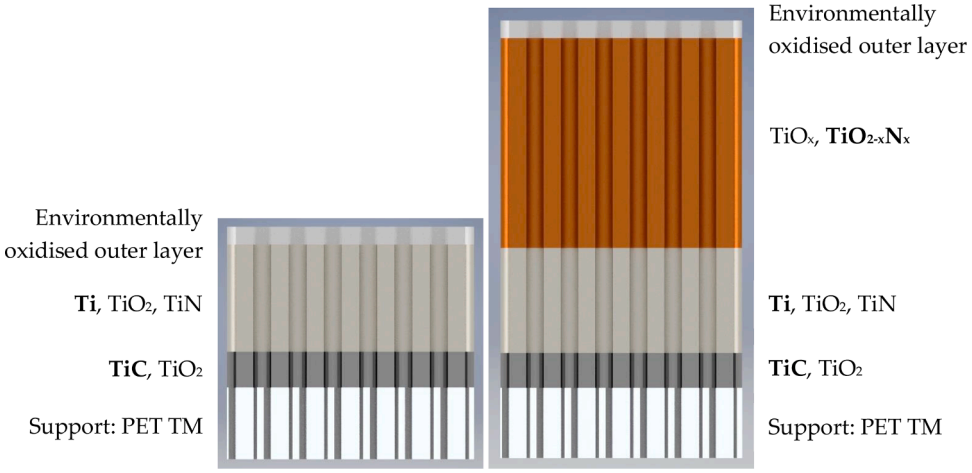

Fig. 9. Illustration of the deposited thin film composition according to the analysis of the data for Ti (left) and Ti-TiO_2 (right). Note that the major component within a later is indicated in bold.

Table 2
Critical load results of Ti and TiO_2-Ti coated TMs.

No.	Sample	*Critical load* L_c, mN	Coefficient of friction m_c at critical load
1	Ti-TM (Fig. 10a)	8.6	0.28
2	Ti-TM (Fig. 10b)	3.8	0.57
3	TiO_2-Ti-TM (Fig 11a)	6.4	0.24
4	TiO_2-Ti-TM (Fig 11b)	3.9	0.59

of the curves obtained for the PET track-etched membranes, both coated and non-coated. The former samples show the typical behaviour of semicrystalline polymers below glass temperature [44]. Also, the pristine and metallized PET films showed significantly higher values of strain and tensile strength compared to track-etched membranes. Therefore, the irradiation by Xe and physicochemical treatment during etching processes drastically changed the tensile behaviour of the PET polymer samples. Considering the fact that the thickness of both types of samples was nearly the same, it can be stated that the decrease in stress and strain was caused by a large number of pores, the presence of which lead to a decrease in the effective cross section of the track membrane sample [45,46] . The maximum stress and maximum strain average

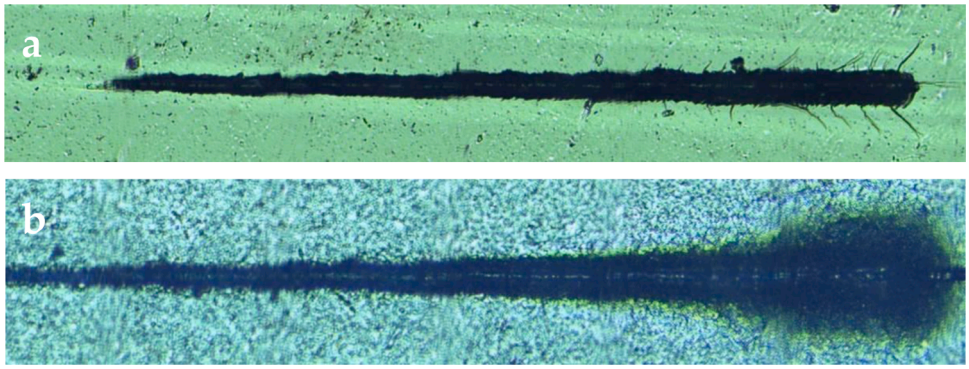

Fig. 10. View of scratches obtained from scratch testing Ti coatings on top of a TM support (a-narrow, b-wide strip scratch).

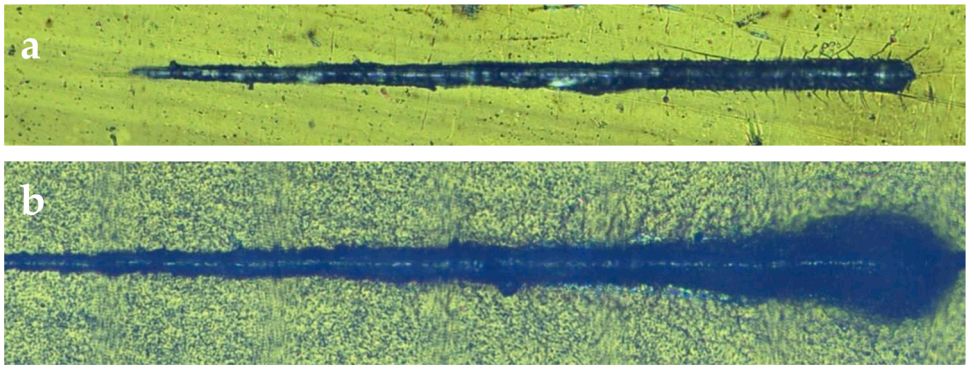

Fig. 11. View of scratches obtained from scratch testing TiO_2-Ti coatings on top of a TM support (a-narrow, b-wide strip scratch).

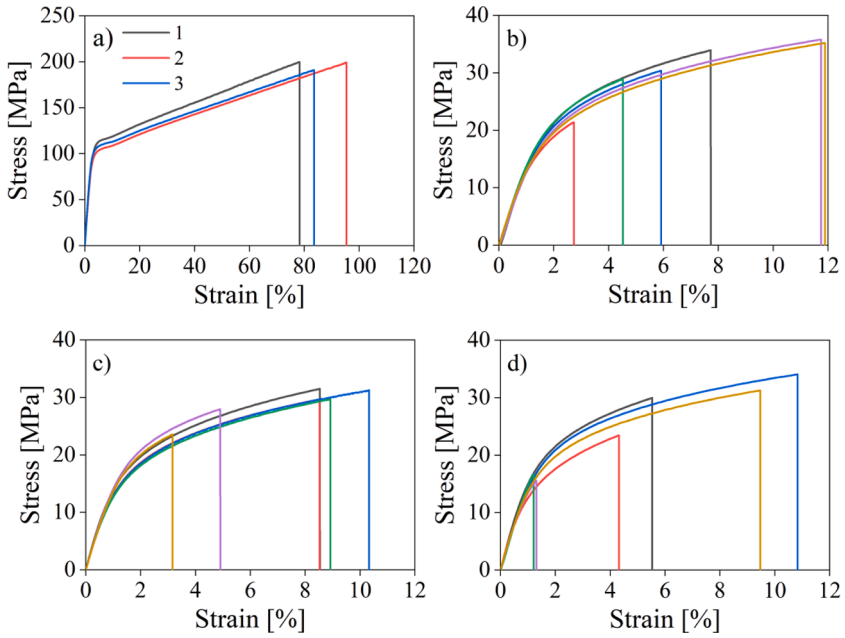

Fig. 12. Stress-strain curves obtained for the investigated samples. (a) Pristine PET foil (1), Ti-coated foil (2) and TiO_2-Ti-coated foil (3). For non-coated track-etched PET membranes (b) and coated by titanium and titanium dioxide membranes (c, d), the results of six independent measurements are presented.

values calculated for the track-etched membranes are presented in Table. 3.

Due to the stochastic distribution of pores, the irradiated and chemically treated samples are less mechanically uniform than pristine PET films. Some pores overlap during the chemical etching and form conjoined pores that weaken the PET film and cause different tensile properties in different locations of the sample. According to the observations made by Cristofari F. et al. [47] pores arranged perpendicular to the stretching direction are responsible for the weakening of the membrane.

The severe conditions of the magnetron sputtering process do not notably deteriorate the TM polymer films' tensile strength. Even though some etching of the TM surface occurs during the first part of sputtering, the loss in maximum stress/strain is most likely due to the diverse pore distribution between samples as is normal when dealing with TMs. Additionally, the adhesion of the coating to the membrane surface holds up well, this can be seen during the stretching of the membranes. Ti and TiO_2/Ti nanotubes deposited on the walls of the pores change shape from circles to ellipses analogous to that observed for empty pores [45].

3.6. Membrane permeability test

It is not easy to characterise the wettability of a porous polymer surface. Nevertheless, by using the recumbent drop method, the contact angle of wetting was ascertained (Fig. 13). The subsequent change in the hydrophilicity of the TM surface before and after sputtering was observed from the results. Ti and TiO_2-Ti sputter coating of the TM surface notably decreased the contact angle with water, the experimental results are summarised in Table 4.

Experimental data show that the TM sample had a contact angle equal to 71.9 ± 0.1°. It indicates surface hydrophobicity, which may be associated with post-radiation oxidation of the polymer and polar groups' appearance on the surface [48]. The change in surface properties after magnetron sputtering was confirmed by the experiment results of the contact angle, on the samples Ti-TM and TiO_2-Ti-TM. When compared with the TM support, Ti and TiO_2-Ti samples are borderline superhydrophilic.

Table 3
Maximum stress and maximum strain average values obtained for the track-etched membranes.

Sample	Max. stress [MPa]	Max. strain [%]
TM	31 ± 5	7.4 ± 3.8
Ti-TM	29 ± 4	7.4 ± 2.7
TiO_2-Ti-TM	25 ± 8	5.4 ± 4.0

It is important to note that the bubble point method is the standard for pore size determination in TMs as well as the origin of the value written in the data sheet that accompanies the membrane. However, unlike SEM, it does not have the visual aspect allowing one to see artefacts or pore narrowing. However, even though the coated TM's pores might seem narrower than the uncoated TM's pores, it does not necessarily mean that the membrane permeability has been negatively affected. That is why the permeability was investigated to understand the filtration properties of coated membranes as well.

According to the SEM analysis of the samples' surface in Section 3.1, it was revealed that the average surface pore diameter is 400 nm ±10%. However, this method does not give a complete insight of the pore geometry along its entire length. Therefore, the water permeability and bubble point methods were investigated to study the pore diameter. The results of the experiment are summarised in Table 5.

With a steady laminar flow of a viscous incompressible liquid through a long cylindrical capillary of circular cross-section, the liquid's volumetric flow rate is directly proportional to the pressure drop per unit of capillary length and the fourth power of the radius. It is inversely proportional to the liquid's viscosity coefficient, which corresponds to the Hagen-Poiseuille law [49].

It should be noted that the gas passing through the dampened membrane will be observed primarily through the largest capillary, also known as the first bubble point. The radius of which can be calculated using the Young-Laplace equation [48,50].

During the experiment of measuring the pore diameter of the studied samples, it was discovered that the sputtering of titanium on the TM surface etches the existing pores. It could have resulted from either the preliminary plasma cleaning of the surface or the material sputtering itself [51,52]. On contact with the treated surface, the chemically active cold plasma causes many physical and chemical processes. The primary reagents of these processes are highly active short-lived chemical compounds produced in large quantities by plasma. It should also be kept in

Fig. 13. Contact angle (a) TM, (b) Ti-TM, (c) TiO_2-Ti-TM.

Table 4
Wetting angle of PET TM and PET TM modified with Ti and TiO_2.

Sample	Contact angle (wetting)
TM	71.9±2
Ti-TM	33.4±2
TiO_2-Ti-TM	28.1±3

Table 5
Pore diameter measured by different methods.

Analytical technique	The pore diameter of the sample, μm		
	TM	Ti-TM	TiO_2-Ti-TM
Water permeability	0.34	0.36	0.35
Bubble point method	0.30	0.32	0.31
SEM (surface)	0.45	0.42	0.39
Margin of error	±10%		

mind that when an electric discharge is in direct contact with a surface, it is also irradiated with ultraviolet radiation and attacked by energetic ions and electrons [53].

In the process of magnetron sputtering, no additional cooling elements were used, which leads to higher temperatures of the sputtered process and supporting surface. According to assumptions made in this study, this crystallises the upper layers of TM and etches the pores. Etching continues until the formation of the primary layer of the sputtered material forms. After that, a gradual layering of the material occurs, during which the pore diameter decreases and the capillary length increases.

The permeability investigation revealed that the Ti-TM samples had the highest transport rate for water. This is directly related to the increase in pore diameter. It is important to note that the TiO_2-Ti-TM samples have similar performance characteristics to the native TM. Simultaneously, TiO_2-Ti-TM had a smaller pore diameter and an increased capillary length (by 140 nm), due to the deposited layer of titanium dioxide. This is shown by the reduced contact angle. In filtering water through a given sample, the liquid wets the pore surface well, resulting in the increased permeability, while maintain the “hour-glass” pore shape as described by Beriozkin V. et al. [54].

4. Conclusions

The large-scale sputter deposition of Ti and TiO_2-Ti thin films on top of PET track-etched membrane supports by industrial roll-to-roll planar magnetron sputtering was investigated. Track-etched membranes were chosen as the porous supporting structure with the idea of being a model and transferring the technology to other membrane processes.

SEM and AFM investigation of the hybrid membrane morphology showed that the Ti and TiO_2-Ti thin films were made up of fused nanoparticles. Based on SEM, the surface pore diameter was slightly reduced when compared to the native TM because of the sputter deposition. However, based on the permeability analysis, this pore size reduction was insufficient to influence the overall filtration performance notably.

XPS and EDS verified the elemental presence of nitrogen in the deposited thin films. Nitrogen was mainly in the form of TiN, resulting from a combination of the degassing of the TM support and the reactive depositing process during the extended low-vacuum sputtering of TiO_2. The appearance of TiC is principally associated with the surface-sputter interaction between the TM support and the initial deposition. The TiC being a by-product of the polymer-Ti interaction during the first few moments of Ti sputtering.

Examining the layer-by-layer composition of the deposited thin-film material and the changes to the TM pore struct gave a new perspective into these thin films’ working characteristics and limitations on top of porous polymer support.

The Ti and TiO_2-Ti coated TMs showed a significant reduction in their contact angle. From 72° for the native TM to 33 and 28° for Ti and TiO_2-Ti for the sputter-coated TM, respectively. The enhanced hydrophilic effect helps improve surface interactions within filtration devices and, in doing so, could reduce surface fouling.

The scratch test showed good adhesion between the TM and sputtered coatings and the tensile test complimented this. Additionally, the tensile test proved that the coating process did not notably weaken the underlying polymeric membrane integrity during sputter deposition despite the slight surface etching. However, a decrease in the tensile strength of the track membranes compared to the native PET film was observed. The TMs are more brittle than the PET films due to the physicochemical treatment of the PET. The slight variance between tensile stress of the coated TM samples is most likely due to the variation in pore density, and the number of overlapping pores in individual samples as each TM is unique.

This investigation confirms that roll-to-roll planar magnetron sputtering of Ti and TiO_2 is a viable strategy for the surface modification of porous polymeric supports such as track-etched membranes on a large scale. Additional research into the challenges of the large-scale surface sputter coating of porous polymeric membranes is recommended. However, it is postulated that hybrid membranes based on these TM model supports could invigorate the TM market and aid the industrial demand for more defined filtration in advanced technologies such as separation, biotechnology, and microelectronics.

Funding

This work was funded by the National Research Foundation and the Department of Science and Innovation of South Africa (grant number 129,274) in association with the Joint Institute for Nuclear Research, Russia. A.O. (XPS and AFM) and K.O. (Tensile test) gratefully acknowledge the financial support by the Plenipotentiary Representative of the Republic of Poland at JINR within the project № 75/44/2020 and grants № 80/12/2020, 80/13/2020.

CRediT authorship contribution statement

Arnoux Rossouw: Conceptualization, Formal analysis, Investigation, Methodology, Project administration, Validation, Visualization, Writing – original draft, Writing – review & editing. **Andrzej Olejniczak:** Investigation, Formal analysis, Software, Writing – review & editing. **Katarzyna Olejniczak:** Investigation, Formal analysis, Writing – review & editing. **Boris Gorberg:** Resources. **Iliya Vinogradov:** Investigation, Writing – review & editing. **Olga Kristavchuk:** Data curation,

Visualization. **Alexander Nechaev:** Supervision, Funding acquisition, Writing – review & editing. **Leslie Petrik:** Supervision, Writing – review & editing. **Willem Perold:** Supervision, Writing – review & editing. **Sergey Dmitriev:** Supervision, Funding acquisition.

Declaration of Competing Interest

"The authors declare no conflict of interest." "The funders had no role in the design of the study; in the collection, analyses, or interpretation of data; in the writing of the manuscript, or in the decision to publish the results".

Acknowledgments

The authors would like to thank O. Mamontov and A. Nikitin from IvTechnoMash LLC as well as *Sc*.D. P. Apel from JINR for their ongoing support during this work.

References

[1] M.N. De Pinho, M. Minhalma, Introduction in Membrane Technologies, Sep. Funct. Mol. Food by Membr. Technol. (2019) 1–29, https://doi.org/10.1016/B978-0-12-815056-6.00001-2.
[2] M. Mulder, Basic Principles of Membrane Technology, Springer, Netherlands, Dordrecht, 1996, https://doi.org/10.1007/978-94-009-1766-8.
[3] M. Yoshida, M. Asano, H. Omichi, R. Spohr, R. Katakai, Substrate-specific functional membranes based on etched ion tracks, Radiat. Meas. 28 (1997) 799–810, https://doi.org/10.1016/S1350-4487(97)00187-X.
[4] S.N. Dmitriev, L.I. Kravets, V.V. Sleptsov, V.M. Elinson, V.V. Potryasai, O. L. Orelovich, High-frequency plasma-discharge effect on poly(ethylene) terephthalate films exposed to heavy ions, Nucl. Instrum. Methods Phys. Res. Sect. B Beam Interact. Mater. Atoms 171 (2000) 448–454, https://doi.org/10.1016/S0168-583X(00)00298-6.
[5] V.A. Pronin, V.N. Gornov, A.V. Lipin, P.A. Loboda, B.V. Mchedlishvili, A. N. Nechaev, A.V. Sergeev, Ion-beam modification of track membrane surface, Tech. Phys. 46 (2001) 1444–1447, https://doi.org/10.1134/1.1418510.
[6] A.V. Sergeev, E.V. Khataibe, V.V. Berezkin, A.N. Nechaev, I.P. Chikhacheva, V. P. Zubov, B.V. Mchedlishvili, Modification of the surfaces of polymer films irradiated by heavy ions and nucleopore nanofilters by XeF2 vapors, Colloid J. Russ. Acad. Sci. 65 (2003) 84–88, https://doi.org/10.1023/A:1022327226695.
[7] A. Bogaerts, E. Neyts, R. Gijbels, J. Van der Mullen, Gas discharge plasmas and their applications, Spectrochim. Acta B 57 (2002) 609–658, https://doi.org/10.1016/S0584-8547(01)00406-2.
[8] Y.G. Shen, Y.W. Mai, Q.C. Zhang, D.R. McKenzie, W.D. McFall, W.E. McBride, Residual stress, microstructure, and structure of tungsten thin films deposited by magnetron sputtering, J. Appl. Phys. 87 (1999) 177, https://doi.org/10.1063/1.371841.
[9] T. Prasanna Kumari, M. Manivel Raja, A. Kumar, S. Srinath, S.V. Kamat, Effect of thickness on structure, microstructure, residual stress and soft magnetic properties of DC sputtered Fe65Co35 soft magnetic thin films, J. Magn. Magn. Mater. 365 (2014) 93–99, https://doi.org/10.1016/J.JMMM.2014.04.030.
[10] A.I. Maksimov, Vacuum-plasma and plasma-solution modification of macromolecular compounds. Potentials and limitations, Khimicheskie Volokna. 36 (2004) 22–25.
[11] N. Khlebnikov, E. Polyakov, S. Borisov, N. Barashev, E. Biramov, A. Maltceva, A. Vereshchagin, S. Khartov, A. Voronin, Composite materials obtained by the ion–plasma sputtering of metal compound coatings on polymer films, Jpn. J. Appl. Phys. 55 (2016) 01AG02, https://doi.org/10.7567/JJAP.55.01AG02.
[12] L. Kravets, A. Gilman, M. Yablokov, V. Elinson, B. Mitu, G. Dinescu, Surface and electrochemical properties of plasma-treated polypropylene track membrane, Plasma Process. Polym. 10 (2013) 603–618, https://doi.org/10.1002/ppap.201200084.
[13] S.C. Park, S.S. Yoon, J.D. Nam, Surface characteristics and adhesive strengths of metal on O_2 ion beam treated polyimide substrate, Thin Solid Films 516 (2008) 3028–3035, https://doi.org/10.1016/J.TSF.2007.11.113.
[14] H. Frey, H.R. Khan, Handbook of Thin-Film Technology, Springer, Berlin Heidelberg, 2015, pp. 1–379.
[15] A. Rossouw, O.V. Artoshina, A.N. Nechaev, P.Y. Apel, L. Petrik, W.J. Perold, C. A. Pineda-Vargas, Stable Ion Beam Analysis (RBS and PIXE) Study of Photocatalytic Track-Etched, Membranes (2015) 591–596, https://doi.org/10.1142/9789814632041_0065.
[16] S.V.A. L'vovich, Gorberg Boris, Ivanov Andrej Anatol'evich, Mamontov Oleg Vladimirovich, PROCEDURE FOR MODIFYING SURFACE OF TEXTILE MATERIAL, RU2398045, n.d.
[17] O.V. Artoshina, F.O. Milovich, A. Rossouw, B.L. Gorberg, L.D. Iskhakova, R. P. Ermakov, V.K. Semina, Y.K. Kochnev, A.N. Nechaev, P.Y. Apel, Structure and phase composition of thin TiO_2 films grown on the surface of metallized track-etched polyethylene terephthalate membranes by reactive magnetron sputtering, Inorg. Mater. 52 (2016) 945–954, https://doi.org/10.1134/S0020168516080021.
[18] T. Tsuchiya, M. Hirata, N. Chiba, Young's modulus, fracture strain, and tensile strength of sputtered titanium thin films, Thin Solid Films 484 (2005) 245–250, https://doi.org/10.1016/j.tsf.2005.02.024.
[19] V. Chawla, R. Jayaganthan, A.K. Chawla, R. Chandra, Microstructural characterizations of magnetron sputtered Ti films on glass substrate, J. Mater. Process. Technol. 209 (2009) 3444–3451, https://doi.org/10.1016/J.JMATPROTEC.2008.08.004.
[20] V. Chawla, R. Jayaganthan, A.K. Chawla, R. Chandra, Microstructural characterizations of magnetron sputtered Ti films on glass substrate, J. Mater. Process. Technol. 209 (2009) 3444–3451, https://doi.org/10.1016/j.jmatprotec.2008.08.004.
[21] O.V. Artoshina, A. Rossouw, V.K. Semina, A.N. Nechaev, P.Y. Apel, Structural and physicochemical properties of titanium dioxide thin films obtained by reactive magnetron sputtering, on the surface of track-etched membranes, Pet. Chem. 55 (2015) 759–768, https://doi.org/10.1134/S0965544115100011.
[22] U. Diebold, The surface science of titanium dioxide, Surf. Sci. Rep. 48 (2003) 53–229, https://doi.org/10.1016/S0167-5729(02)00100-0.
[23] O. CARP, Photoinduced reactivity of titanium dioxide, Prog. Solid State Chem. 32 (2004) 33–177, https://doi.org/10.1016/j.progsolidstchem.2004.08.001.
[24] A. Fujishima, T.N. Rao, D.A. Tryk, Titanium dioxide photocatalysis, J. Photochem. Photobiol. C Photochem. Rev. 1 (2000) 1–21, https://doi.org/10.1016/S1389-5567(00)00002-2.
[25] X. Chen, S.S. Mao, Titanium dioxide nanomaterials–Synthesis, properties, modifications and applications, Chem. Rev. 107 (2007) 2891–2959, https://doi.org/10.1021/cr0500535.
[26] J. Zhang, P. Zhou, J. Liu, J. Yu, New understanding of the difference of photocatalytic activity among anatase, rutile and brookite TiO_2, Phys. Chem. Chem. Phys. 16 (2014) 20382–20386, https://doi.org/10.1039/c4cp02201g.
[27] Y.M. Sung, H.J. Kim, Sputter deposition and surface treatment of TiO_2 films for dye-sensitized solar cells using reactive RF plasma, Thin Solid Films 515 (2007) 4996–4999, https://doi.org/10.1016/j.tsf.2006.10.079.
[28] A.L. Linsebigler, G. Lu, J.T. Yates, Photocatalysis on TiO_2 surfaces–Principles, mechanisms, and selected results, Chem. Rev. 95 (1995) 735–758, https://doi.org/10.1021/cr00035a013.
[29] G.N. Flerov, P.Y. Apel', A.Y. Didyk, V.I. Kuznetsov, R.T. Oganesyan, Use of heavy-ion accelerators to produce nuclear membranes, Sov. At. Energy. 67 (1989) 763–770. doi:10.1007/BF01123341.
[30] P.Y. Apel, S.N. Dmitriev, Micro- and nanoporous materials produced using accelerated heavy ion beams, Adv. Nat. Sci. Nanosci. Nanotechnol. 2 (2011), 013002, https://doi.org/10.1088/2043-6262/2/1/013002.
[31] Ivtechnomash–Film metallization, fabrics metallization, (n.d.). http://en.ivtechnomash.ru/ (accessed January 21, 2021).
[32] B.L. Gorberg, A.A. Ivanov, O.V. Mamontov, V.A. Stegnin, V.A. Titov, Modification of textile materials by the deposition of nanocoatings by magnetron ion-plasma sputtering, Russ. J. Gen. Chem. 83 (2013) 157–163, https://doi.org/10.1134/S1070363213010350.
[33] A. Rossouw, O. Kristavchuk, A. Olejniczak, C. Bode-Aluko, B. Gorberg, A. Nechaev, L. Petrik, W. Perold, P. Apel, Modification of polyethylene terephthalate track etched membranes by planar magnetron sputtered Ti/TiO_2 thin films, Thin Solid Films (2021), 138641, https://doi.org/10.1016/j.tsf.2021.138641.
[34] A.B. Solovieva, V.A. Timofeeva, N.A. Erina, G.V. Vstovsky, A.V. Krivandin, O. V. Shatalova, P.Y. Apel', B.V. McHedlishvili, S.F. Timashev, Peculiarities of the formation of track-etched membranes by the data of atomic force microscopy and X-ray scattering, Colloid J. 67 (2005) 217–226, https://doi.org/10.1007/s10595-005-0084-6.
[35] F. Dinelli, H.E. Assender, K. Kirov, O.V. Kolosov, Surface morphology and crystallinity of biaxially stretched PET films on the nanoscale, Polymer (Guildf) 41 (2000) 4285–4289, https://doi.org/10.1016/S0032-3861(99)00500-5.
[36] E. Wohlfart, J.P. Fernández-Blázquez, E. Knoche, A. Bello, E. Pérez, E. Arzt, A. Del Campo, Nanofibrillar patterns by plasma etching–The influence of polymer crystallinity and orientation in surface morphology, Macromolecules 43 (2010) 9908–9917, https://doi.org/10.1021/ma101889s.
[37] K. Teshima, H. Sugimura, Y. Inoue, O. Takai, A. Takano, Ultra-water-repellent poly(ethylene terephthalate) substrates, Langmuir 19 (2003) 10624–10627, https://doi.org/10.1021/la034265d.
[38] P. Jiang, S. Geng, X. Shao, G. Mi, C. Wang, H. Wu, C. Han, S. Gao, Fine grains reduce cracking susceptibility during solidification–Insights from phase-field simulations, JOM 71 (2019) 3223–3229, https://doi.org/10.1007/s11837-019-03342-w.
[39] W. Göpel, J.A. Anderson, D. Frankel, M. Jaehnig, K. Phillips, J.A. Schäfer, G. Rocker, Surface defects of TiO_2(110)–A combined XPS, XAES AND ELS study, Surf. Sci. 139 (1984) 333–346, https://doi.org/10.1016/0039-6028(84)90054-2.
[40] M.C. Biesinger, L.W.M. Lau, A.R. Gerson, R.S.C. Smart, Resolving surface chemical states in XPS analysis of first row transition metals, oxides and hydroxides–*Sc*, Ti, V, Cu and Zn, Appl. Surf. Sci. 257 (2010) 887–898, https://doi.org/10.1016/j.apsusc.2010.07.086.
[41] A. Rossouw, O. Kristavchuk, A. Olejniczak, C. Bode-Aluko, B. Gorberg, A. Nechaev, L. Petrik, W. Perold, P. Apel, Modification of polyethylene terephthalate track etched membranes by planar magnetron sputtered Ti/TiO_2 thin films, Thin Solid Films 725 (2021), 138641, https://doi.org/10.1016/j.tsf.2021.138641.
[42] E. Lewin, P.O... Persson, M. Lattemann, M. Stüber, M. Gorgoi, A. Sandell, C. Ziebert, F. Schäfers, W. Braun, J. Halbritter, S. Ulrich, W. Eberhardt, L. Hultman, H. Siegbahn, S. Svensson, U. Jansson, On the origin of a third spectral component of C1s XPS-spectra for nc-TiC/a-C nanocomposite thin films, Surf. Coat. Technol. 202 (2008) 3563–3570, https://doi.org/10.1016/j.surfcoat.2007.12.038.

[43] D. Jaeger, J. Patscheider, A complete and self-consistent evaluation of XPS spectra of TiN, J. Electron Spectrosc. Relat. Phenom. 185 (2012) 523–534, https://doi.org/10.1016/j.elspec.2012.10.011.
[44] R. Janssen, Deformation and failure in semi-crystalline polymer systems, 2002.
[45] V.N. Gumirova, G.S. Abdurashidova, S.A. Bedin, N.P. Zabalueva, M.A. Kuvaitseva, I.V. Razumovskaya, Specific features of the fracture of track membranes and related polymer/metal composites prepared by template synthesis, Phys. Solid State 57 (2015) 344–348, https://doi.org/10.1134/S1063783415020134.
[46] L.S. Worrel, Modification of track-etched membrane structure and performance via uniaxial stretching, 2005.
[47] F. Cristofari, B. Piotrowski, R. Pesci, Mechanical properties of a nanoporous membrane used in implantable medical devices. Correlation between experimental characterization and 2D numerical simulation, J. Mech. Behav. Biomed. Mater. 74 (2017) 43–53, https://doi.org/10.1016/j.jmbbm.2017.05.021.
[48] S.N. Akimenko, P.Y. Apel, M. Ioshida, T.I. Mamonova, J. Maekawa, O.L. Orelovich, Properties of polyethylene naphthalate track membranes, (2002). https://cds.cern.ch/record/589646 (accessed January 28, 2021).
[49] B. Sartowska, W. Starosta, P. Apel, O. Orelovitch, I. Blonskaya, Polymeric track etched membranes application for advanced porous structures formation, 123 (2013). doi:10.12693/APhysPolA.123.819.
[50] N. Kononenko, V. Nikonenko, D. Grande, C. Larchet, L. Dammak, M. Fomenko, Y. Volfkovich, Porous structure of ion exchange membranes investigated by various techniques, Adv. Colloid Interface Sci. 246 (2017) 196–216, https://doi.org/10.1016/j.cis.2017.05.007.
[51] S.N. Dmitriev, L.I. Kravets, V.V. Sleptsov, Modification of track membrane structure by plasma etching, Nucl. Instrum. Methods Phys. Res. Sect. B Beam Interact. Mater. Atoms 142 (1998) 43–49, https://doi.org/10.1016/S0168-583X(98)00203-1.
[52] L.I. Kravets, S.N. Dmitriev, V.V. Sleptsov, V.M. Elinson, Production of asymmetric track membranes with a high permeability and separation selectivity, Desalination 144 (2002) 27–34, https://doi.org/10.1016/S0011-9164(02)00284-9.
[53] L.G. Molokanova, Y.K. Kochnev, A.N. Nechaev, S.N. Chukova, P.Y. Apel, Effect of ultraviolet radiation on polyethylene naphthalate films irradiated with high-energy heavy ions, High Energy Chem. 51 (2017) 197–203, https://doi.org/10.1134/S0018143917030109.
[54] V.V. Beriozkin, D.L. Zagorsky, A.N. Nechaev, T.V. Tsiganova, N.V. Mitrofanova, P. Y.U. Apel, B.V. McHedlishvili, The track membrane porous structure and selective properties investigation, Radiat. Meas. 34 (2001) 593–595, https://doi.org/10.1016/S1350-4487(01)00235-9.